

ELECTRONIC SUPPLEMENTARY INFORMATION

**Nickel Dimethyl Glyoximato Complex to Form Nickel Based
Nanoparticles for Electrocatalytic H₂ Production**

Stéphanie Cherdo,^a Sanae El Ghachtouli,^a Marie Sircoglou,^a François Brisset,^a Maylis Orio^b and Ally Aukauloo^{a,c}

^a *Institut de Chimie Moléculaire et des Matériaux d'Orsay, UMR-CNRS 8182, Université Paris-Sud XI, F-91405 Orsay, France.*

^b *Laboratoire de Spectrochimie Infrarouge et Raman, UMR-CNRS 8516, Université Lille 1, Sciences et Technologies, F-59655 Villeneuve d'Ascq Cedex - France*

^c *CEA, iBiTec-S, Service de Bioénergétique Biologie Structurale et Mécanismes (SB2SM), F-91191 Gif-sur-Yvette, France.*

Table of Contents

Experimental details (p iii-v)

- Fig. S1** Cyclic voltammograms at different scan rates of $[\text{Ni}(\text{DMGBF}_2)_2]$
- Sch. S1** Possible mechanism involved in the first reduction process of $[\text{Ni}(\text{DMGBF}_2)_2]$
- Fig. S2** Spectroelectrochemical study of complex $[\text{Ni}(\text{DMGBF}_2)_2]$
- Fig. S3** EPR spectrum after electrolysis of complex $[\text{Ni}(\text{DMGBF}_2)_2]$ at -0.85 V
- Fig. S4** Dependence of i_p/i_{p0} at -0.74 V vs. SCE upon addition of HClO_4
- Fig. S5** EDX analysis of the particles deposited
- Fig. S6** Comparison of the catalytic activity of carbon electrodes modified upon electrolysis of $\text{Ni}(\text{DMGBF}_2)_2$ and $\text{Ni}(\text{NO}_3)_2$ solutions

Computational details (p vi-xiv)

- Table S1** Calculated electronic excitations of the monoreduced species
- Table S2** Selected calculated bond lengths for $[\text{Ni}(\text{DMGBF}_2)_2]$ and $[\text{Ni}(\text{DMGBF}_2)_2]^-$
- Table S3** Mulliken spin population analysis of the monoreduced species
- Table S4** Calculated Gibbs free energies for the single protonation
- Table S5** Calculated Gibbs free energies for the double protonation
- Table S6** Calculated Gibbs free energies for the triple protonation
- Table S7** Calculated Gibbs free energies for the quadruple protonation
- Fig. S7** TDDFT assignment of the UV-Vis bands for the monoreduced species $[\text{Ni}(\text{DMGBF}_2)_2]^-$.
- Fig. S8** DFT optimized structure of complex $[\text{Ni}(\text{DMGBF}_2)_2]$ and selected bond distances.
- Fig. S9** DFT optimized structure of the monoreduced species $[\text{Ni}(\text{DMGBF}_2)_2]^-$ and selected bond distances.
- Fig. S10** Highest Occupied Molecular Orbital and Lowest Unoccupied Molecular Orbital for complex $[\text{Ni}(\text{DMGBF}_2)_2]$.
- Fig. S11** Spin density plot and localized SOMO for the monoreduced species $[\text{Ni}(\text{DMGBF}_2)_2]^-$.
- Fig. S12** DFT optimized structures of the doubly protonated species of $[\text{Ni}(\text{DMGBF}_2)_2]^-$.
- Fig. S13** DFT optimized structures of the triply protonated species of $[\text{Ni}(\text{DMGBF}_2)_2]^-$.
- Fig. S14** DFT optimized structures of the quadruply protonated species of $[\text{Ni}(\text{DMGBF}_2)_2]^-$.

Experimental details

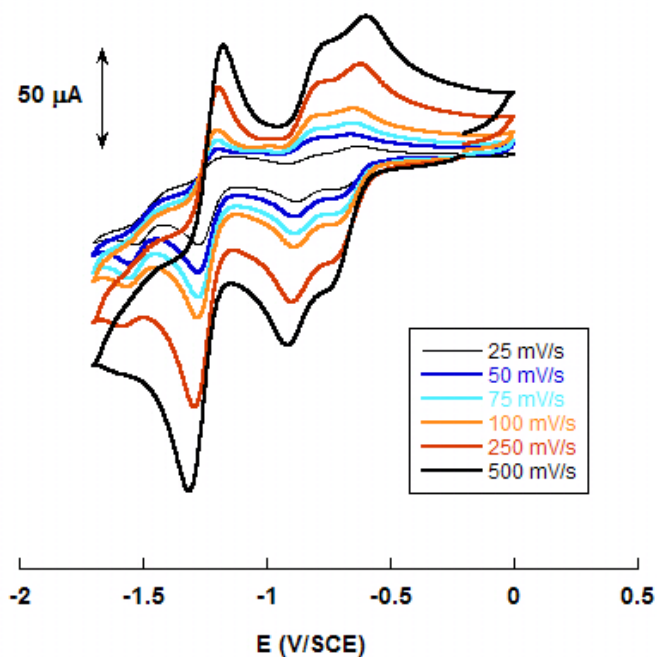
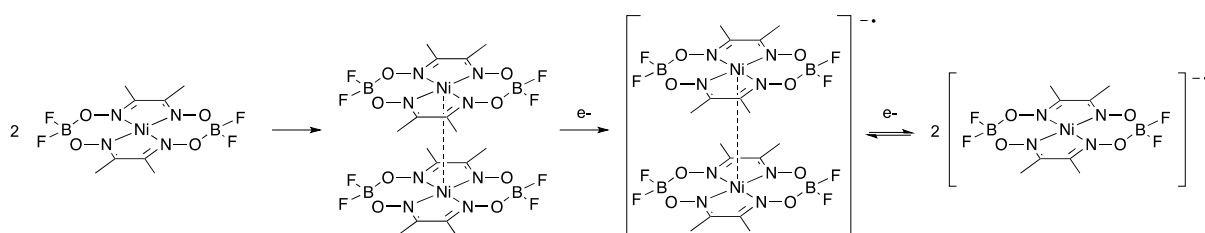


Fig. S1 Cyclic voltammograms at different scan rates of [Ni(DMGBF₂)₂] complex (2mM) in DMF (0.1 M TBAPF₆) at a glassy carbon electrode



Scheme S1 Possible mechanism involved in the first reduction process of [Ni(DMGBF₂)₂]

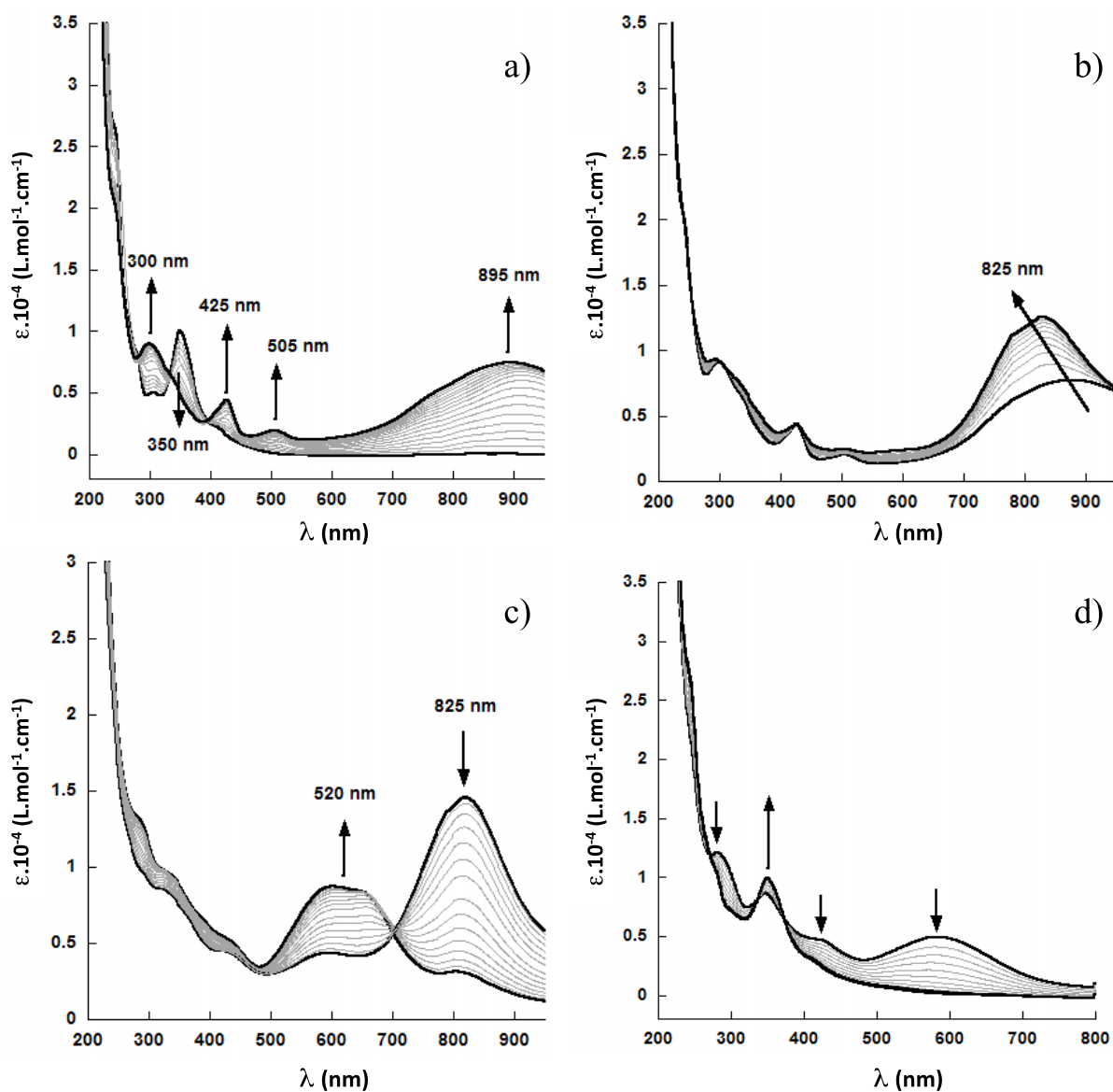


Fig. S2 Spectroelectrochemical study of complex $[\text{Ni}(\text{DMGBF}_2)_2]$: Transient UV-vis spectra recorded during chronoamperometric experiments in reduction ($E = -1.0 \text{ V}$ (a, b), -1.5 V (c) vs. SCE) then oxidation ($E = -0.1 \text{ V vs. SCE}$).

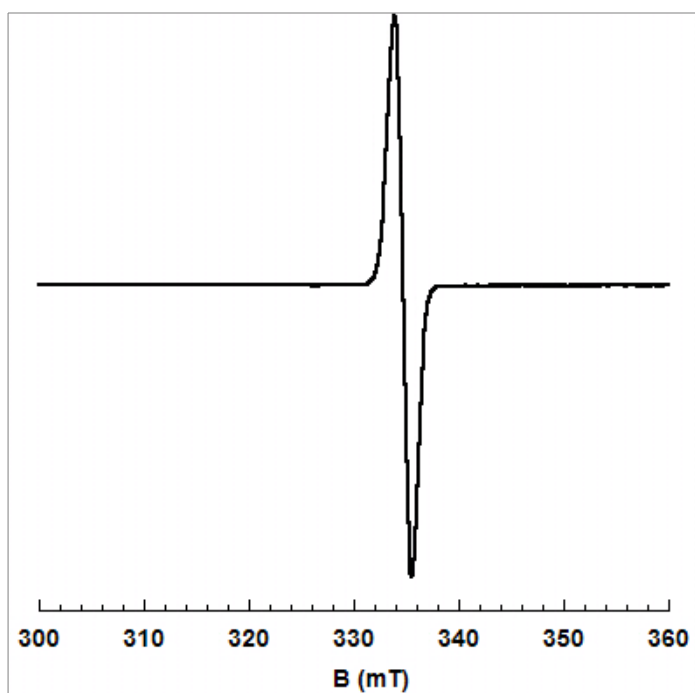


Fig. S3 EPR spectrum after electrolysis of complex $[\text{Ni}(\text{DMGBF}_2)_2]$ at -0.85 V vs. SCE, $T = 100\text{K}$, $\nu = 9.4$ GHz ; $g = 2.00$.

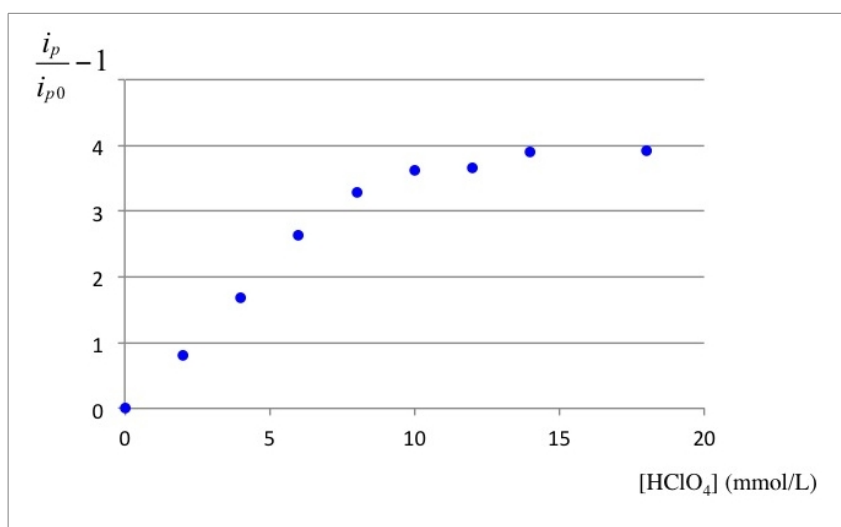


Fig. S4 Dependence of i_p/i_{p0} at -0.74 V vs. SCE upon addition of HClO_4 to a solution of $[\text{Ni}(\text{DMGBF}_2)_2]$ in DMF (complex: 2mM, NaClO_4 : 0.1 M, $\nu = 0.1$ V/s, working electrode : glassy carbon electrode)

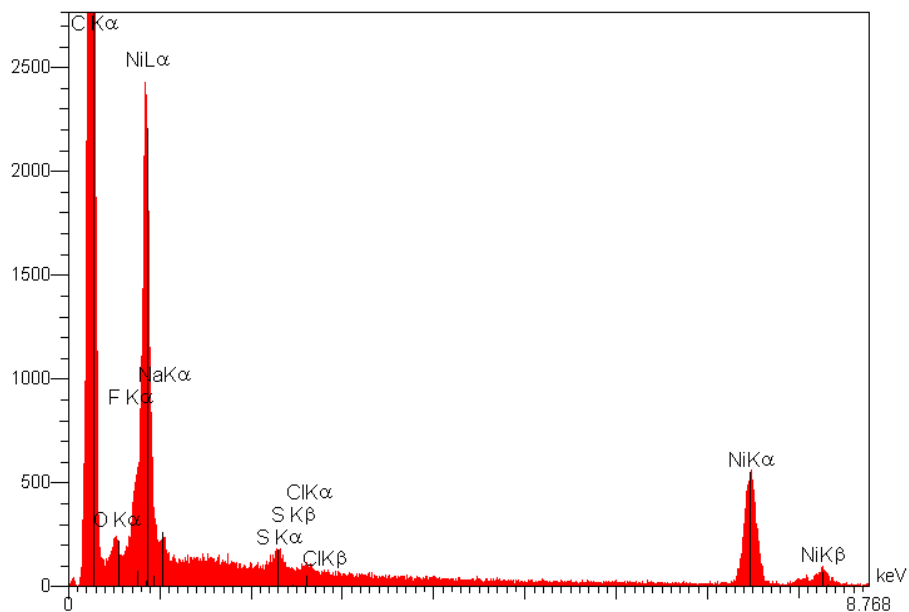


Fig. S5 EDX analysis of the particles deposited onto a 1 cm² glassy carbon surface after the 16h electrolysis ($E = -0.8$ V vs SCE) of a solution (S) of $[\text{Ni}(\text{DMGBF}_2)_2]$ in DMF (complex : 2 mM, NaClO_4 : 0.1 M, HClO_4 : 18 mM)

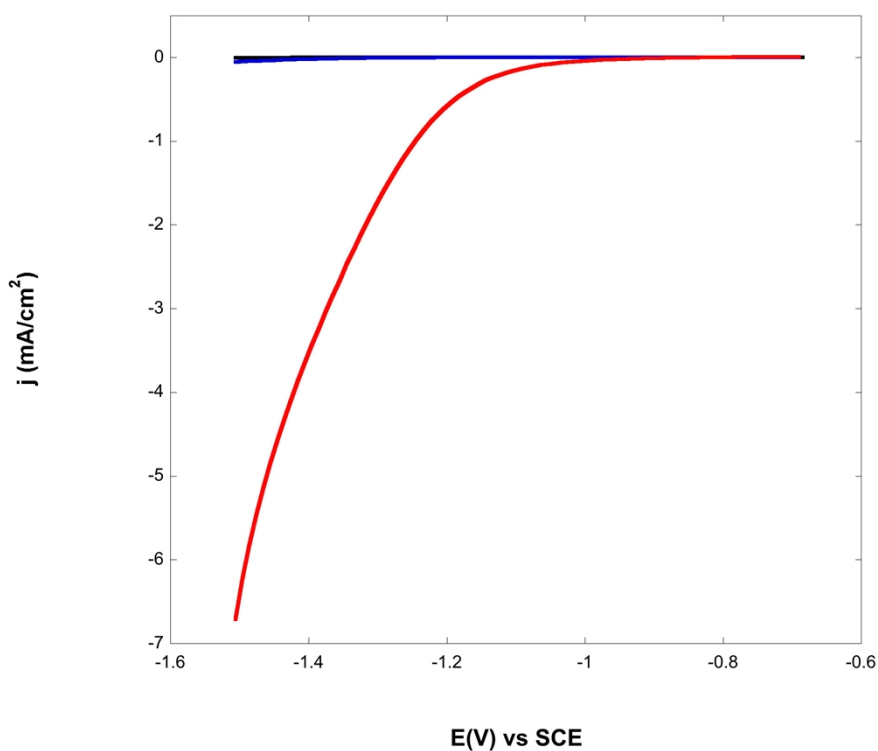


Fig. S6 CV in water at pH 7 ($\text{KH}_2\text{PO}_4/\text{K}_2\text{HPO}_4$: 0,1 M, NaClO_4 : 0.1M, $v = 0.1$ V/s) of **Black** : a bare glassy carbon electrode; **Blue** : a glassy carbon electrode modified after electrolysis (-1 V vs SCE) of a $\text{Ni}(\text{NO}_3)_2$ solution (2 mM, NaClO_4 : 0.1 M, HClO_4 : 20 mM); **Red** : a glassy carbon electrode modified after electrolysis (-0.8 V vs SCE) of a $[\text{Ni}(\text{DMGBF}_2)_2]$ solution (2 mM, NaClO_4 : 0.1 M, HClO_4 : 18 mM)

Computational details

All theoretical calculations were performed with the ORCA program package.¹ Full geometry optimizations were carried out for all complexes using the GGA functional BP86²⁻⁴ in combination with the TZV/P⁵ basis set for all atoms and by taking advantage of the resolution of the identity (RI) approximation in the Split-RI-J variant⁶ with the appropriate Coulomb fitting sets.⁷ Increased integration grids (Grid4 in ORCA convention) and tight SCF convergence criteria were used. Solvent effects were accounted for according to the experimental conditions. For that purpose, we used the DMF ($\epsilon = 38$) solvent within the framework of the conductor like screening (COSMO) dielectric continuum approach.⁸ The relative energies were obtained from single-point calculations using the B3LYP^{9,10} functional together with the TZV/P basis set. They were computed from the gas-phase optimized structures as a sum of electronic energy, thermal corrections to free energy, and free energy of solvation. Optical properties were predicted from additional single-point calculations using the same functional/basis set as employed before. Electronic transition energies and dipole moments for all models were calculated using time-dependent DFT (TD-DFT)¹¹⁻¹³ within the Tamm-Dancoff approximation.^{14,15} To increase computational efficiency, the RI approximation¹⁶ was used in calculating the Coulomb term and at least 30 excited states were calculated in each case.

The DFT-optimised structure of the original nickel(II) DMG complex is in good accord with the experimental X-ray data²² (Table S2 and Fig. S8). A comparison of the metric distances of the neutral and monoreduced species indicates only a feeble shrinking in the metal-coordinating nitrogen atoms of about 0.03 Å (Table S2). However, the ligand skeleton undergoes quite noticeable changes as depicted in Figs. S7 and S8. The spin density plot as well as the Singly Occupied Molecular Orbital (SOMO) for the monoreduced $[\text{Ni}(\text{DMGBF}_2)_2]^-$ are depicted in Fig. S7. Mulliken population analysis of the species shows that the spin density is mainly distributed over the ligand skeleton with a minor contribution from the nickel ion (Table S3). Not surprisingly, the SOMO of $[\text{Ni}(\text{DMGBF}_2)_2]^-$ is almost exclusively distributed over the diiminic fragments with a composition similar to the LUMO of the original complex $[\text{Ni}(\text{DMGBF}_2)_2]$ (Fig. S11).

References

1. Neese, F. *Wiley Interdiscip. Rev. Comput. Mol. Sci.* **2012**, *2*, 73.
2. Perdew, J. P. *Phys. Rev. B* **1986**, *33*, 8822.
3. Perdew, J. P. *Phys. Rev. B* **1986**, *34*, 7406.
4. Becke, A. D. *Phys. Rev. A* **1988**, *38*, 3098.
5. Schäfer, A.; Huber, C.; Ahlrichs, R. *J. Chem. Phys.* **1994**, *100*, 5829.
6. Neese, F. *J. Comput. Chem.* **2003**, *24*, 1740.
7. Weigend, F. *PhysChemChemPhys* **2006**, *8*, 1057.
8. Klamt, A.; Schürmann, G. J. *Chem. Soc., Perkin Trans. 2* **1993**, 799.
9. Becke, A. D. *J. Chem. Phys.* **1993**, *98*, 1372.
10. Lee, C. T.; Yang, W. T.; Parr, R. G. *Phys. Rev. B* **1988**, *37*, 785.
11. Casida, M. E., In *Recent Advances in Density Functional Methods*, Chong, D.P. Ed. World Scientific: Singapore, **1995**.
12. Stratmann, R. E.; Scuseria, G. E.; Frisch, M. J., *J. Chem. Phys.* **1998**, *109*, 8218-8224.
13. Bauernschmitt, R.; Ahlrichs, R., *Chem. Phys. Lett.* **1996**, 454-464.
14. Hirata, S.; Head-Gordon, M., *Chem. Phys. Lett.* **1999**, *314*, 291-299.
15. Hirata, S.; Head-Gordon, M., *Chem. Phys. Lett.* **1999**, *302*, 375-382.

Table S1 Calculated electronic excitations of the monoreduced species $[\text{Ni}(\text{DMGBF}_2)_2]^-$.

λ^{exp} [nm]	λ^{theo} [nm]	f	Assignment	Transition
825 (1.25)	848	0.168	MLCT	$\beta\text{HOMO} \rightarrow \beta\text{LUMO}$
505 (0.25)	460	0.005	LLCT	$\beta\text{HOMO} \rightarrow \beta\text{LUMO}+2$
425 (0.50)	406	0.007	LLCT	$\beta\text{HOMO}-1 \rightarrow \beta\text{LUMO}+1$
300 (1.00)	337	0.179	MLCT	$\beta\text{HOMO}-3 \rightarrow \beta\text{LUMO}$

Table S2 Selected calculated bond lengths for $[\text{Ni}(\text{DMGBF}_2)_2]$ and $[\text{Ni}(\text{DMGBF}_2)_2]^-$.

Bond	$[\text{Ni}(\text{DMGBF}_2)_2]$	$[\text{Ni}(\text{DMGBF}_2)_2]^-$
Ni-N1	1.868	1.835
Ni-N2	1.867	1.835
O1-N1	1.347	1.366
N1-C1	1.299	1.326
C1-C2	1.480	1.442
C2-N2	1.300	1.327
N2-O2	1.347	1.367

Table S3 Mulliken spin population analysis of the monoreduced species $[\text{Ni}(\text{DMGBF}_2)_2]^-$.

Center	Ni	N1	N2	N3	N4	C1	C2
Spin pop.	0.029	0.104	0.111	0.105	0.112	0.117	0.106

Center	C3	C4	O1	O2	O3	O4
Spin pop.	0.117	0.107	0.014	0.016	0.014	0.016

Table S4 Calculated Gibbs free energies for the single protonation of $[\text{Ni}(\text{DMGBF}_2)_2]^-$ ($\text{AH} = \text{HClO}_4$).

Locus	Reaction	ΔG (kcal/mol ⁻¹)	ΔG_{rel} (kcal/mol ⁻¹)
Ni	$[\text{Ni}(\text{L})_2]^- + \text{AH} \rightarrow [\text{Ni}(\text{H})(\text{L})_2] + \text{A}^-$	12.1	36.4
N	$[\text{Ni}(\text{L})_2]^- + \text{AH} \rightarrow [\text{Ni}(\text{L})_2(\text{H}_\text{N})] + \text{A}^-$	-16.3	8.0
C	$[\text{Ni}(\text{L})_2]^- + \text{AH} \rightarrow [\text{Ni}(\text{L})_2(\text{H}_\text{C})] + \text{A}^-$	-24.3	0

Table S5 Calculated Gibbs free energies for the double protonation of $[\text{Ni}(\text{DMGBF}_2)_2]^-$.

Locus	Reaction	ΔG (kcal/mol ⁻¹)	ΔG_{rel} (kcal/mol ⁻¹)
C/N	$[\text{Ni}(\text{L})_2(\text{H}_\text{C})]^- + \text{AH} \rightarrow [\text{Ni}(\text{L})_2(\text{H}_\text{N})(\text{H}_\text{C})] + \text{A}^-$	+6.5	29.9
N/C	$[\text{Ni}(\text{L})_2(\text{H}_\text{N})]^- + \text{AH} \rightarrow [\text{Ni}(\text{L})_2(\text{H}_\text{C})(\text{H}_\text{N})] + \text{A}^-$	-1.4	22.0
2N	$[\text{Ni}(\text{L})_2(\text{H}_\text{N})]^- + \text{AH} \rightarrow [\text{Ni}(\text{L})_2(2\text{H}_\text{N})] + \text{A}^-$	-15.4	8.0
2C	$[\text{Ni}(\text{L})_2(\text{H}_\text{C})]^- + \text{AH} \rightarrow [\text{Ni}(\text{L})_2(2\text{H}_\text{C})] + \text{A}^-$	-23.4	0

Table S6 Calculated Gibbs free energies for the triple protonation of $[\text{Ni}(\text{DMGBF}_2)_2]^-$.

Locus	Reaction	ΔG (kcal/mol ⁻¹)	ΔG_{rel} (kcal/mol ⁻¹)
3N	$[\text{Ni}(\text{L})_2(2\text{H}_\text{N})]^- + \text{AH} \rightarrow [\text{Ni}(\text{L})_2(3\text{H}_\text{N})] + \text{A}^-$	-12.4	13.2
3C	$[\text{Ni}(\text{L})_2(2\text{H}_\text{C})]^- + \text{AH} \rightarrow [\text{Ni}(\text{L})_2(3\text{H}_\text{C})] + \text{A}^-$	-25.6	0

Table S7 Calculated Gibbs free energies for the quadruple protonation of $[\text{Ni}(\text{DMGBF}_2)_2]^-$.

Locus	Reaction	ΔG (kcal/mol ⁻¹)	ΔG_{rel} (kcal/mol ⁻¹)
4N (2)	$[\text{Ni}(\text{L})_2(3\text{H}_\text{N})]^- + \text{AH} \rightarrow [\text{Ni}(\text{L})_2(4\text{H}_\text{N})] + \text{A}^-$	+34.3	58.3
4N (1)	$[\text{Ni}(\text{L})_2(3\text{H}_\text{N})]^- + \text{AH} \rightarrow [\text{Ni}(\text{L})_2(4\text{H}_\text{N})] + \text{A}^-$	+33.2	56.2
4C (2)	$[\text{Ni}(\text{L})_2(3\text{H}_\text{C})]^- + \text{AH} \rightarrow [\text{Ni}(\text{L})_2(4\text{H}_\text{C})] + \text{A}^-$	-21.9	2.1
4C (1)	$[\text{Ni}(\text{L})_2(3\text{H}_\text{C})]^- + \text{AH} \rightarrow [\text{Ni}(\text{L})_2(4\text{H}_\text{C})] + \text{A}^-$	-24.0	0

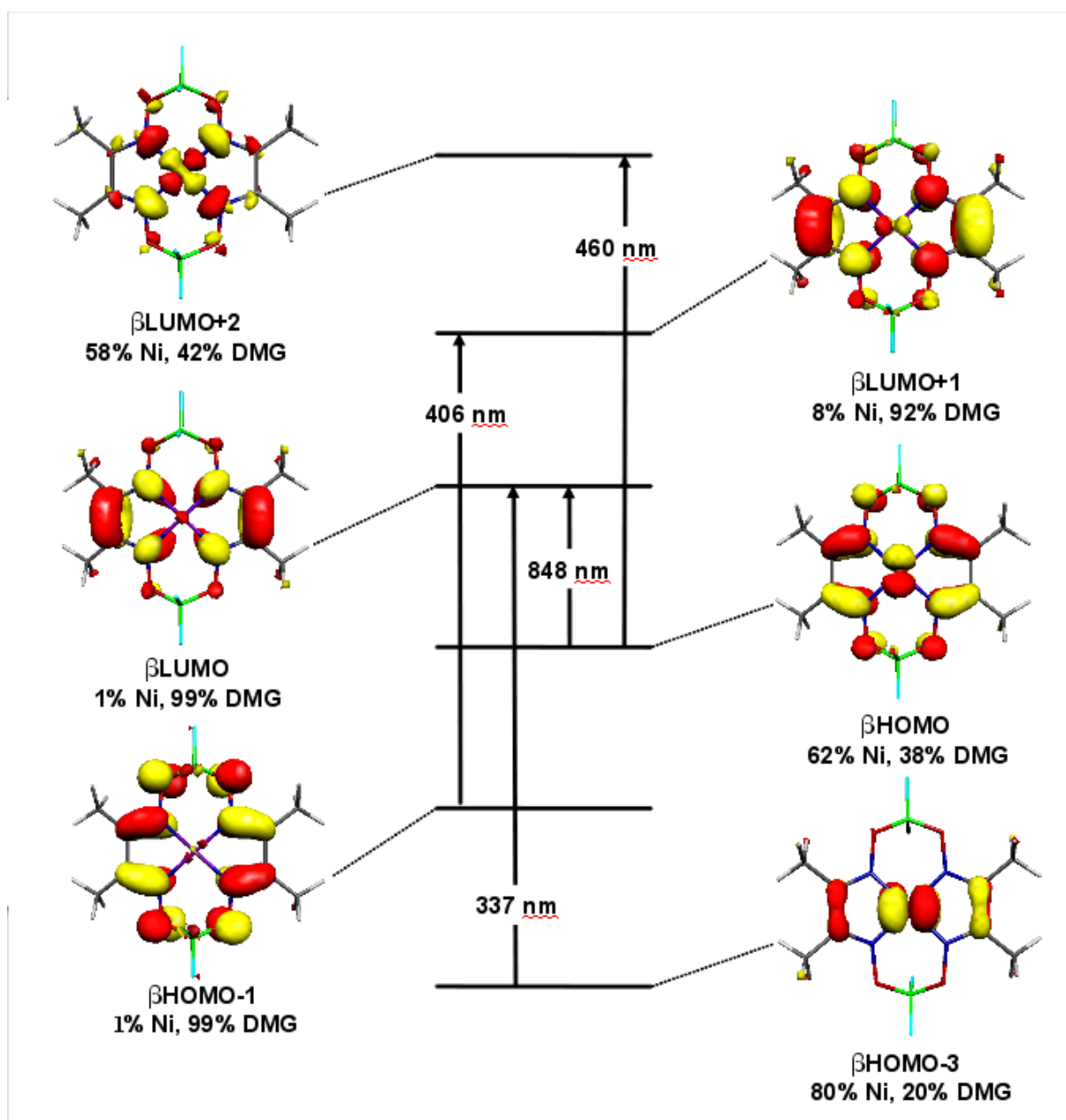


Fig. S7 TDDFT assignment of the UV-Vis bands for the monoreduced species $[\text{Ni}(\text{DMGBF}_2)_2]^-$. The relevant MOs are indicated as well as the wavelength of the optical transitions. Color scheme: Ni: purple, O: red; N: dark blue; C: green and H: white.

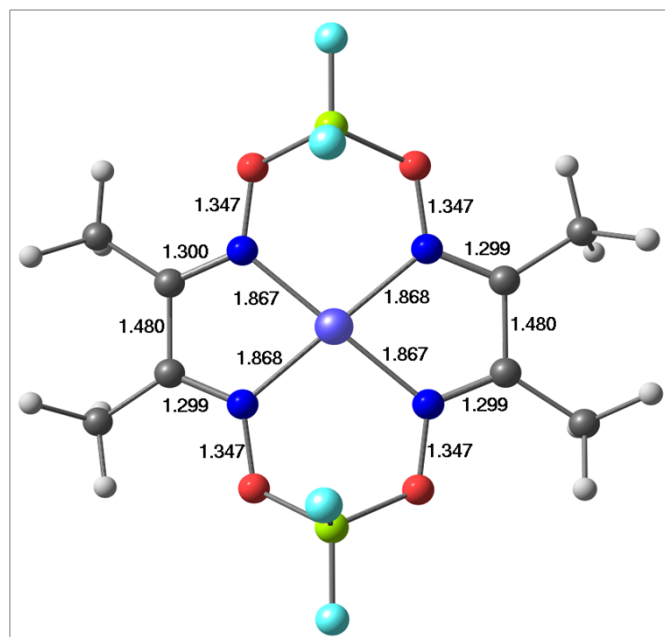


Fig. S8 DFT optimized structure of complex [Ni(DMGBF₂)₂] and selected bond distances. Color scheme: Ni: purple, O: red; N: dark blue; C: green and H: white.

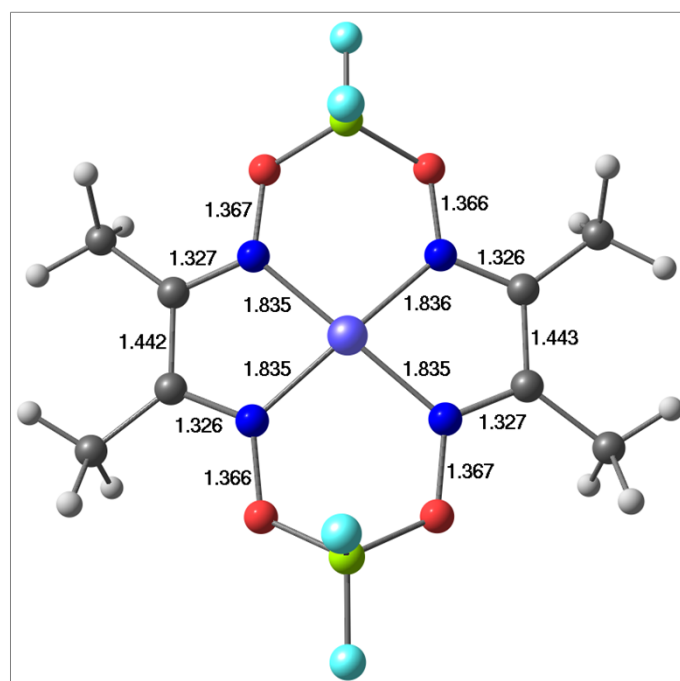


Fig. S9 DFT optimized structure of the monoreduced species [Ni(DMGBF₂)₂]⁻ and selected bond distances.

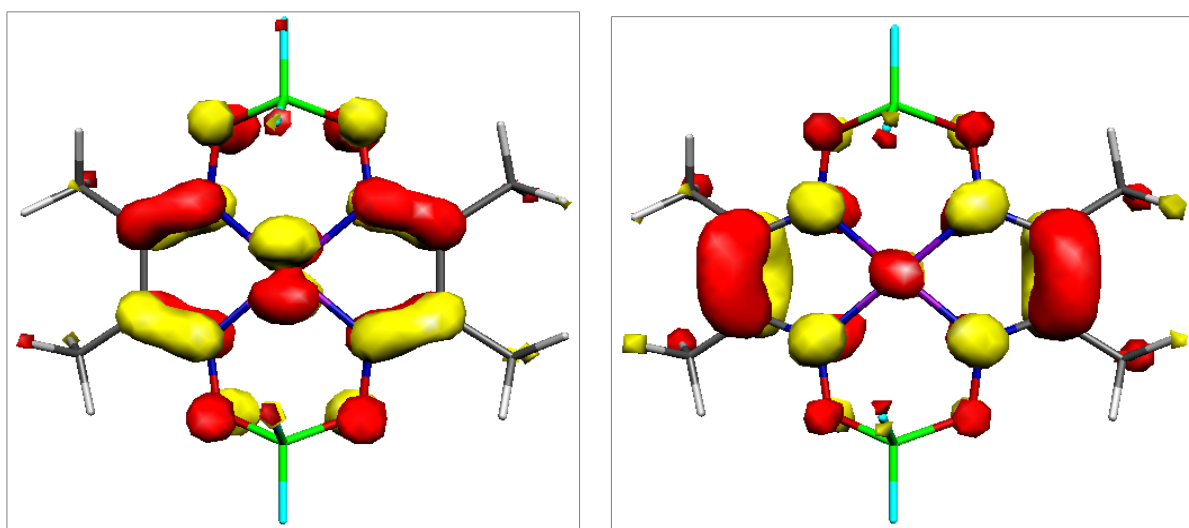


Fig. S10 Highest Occupied Molecular Orbital (HOMO, left) and Lowest Unoccupied Molecular Orbital (LUMO, right) for complex $[\text{Ni}(\text{DMGBF}_2)_2]$.

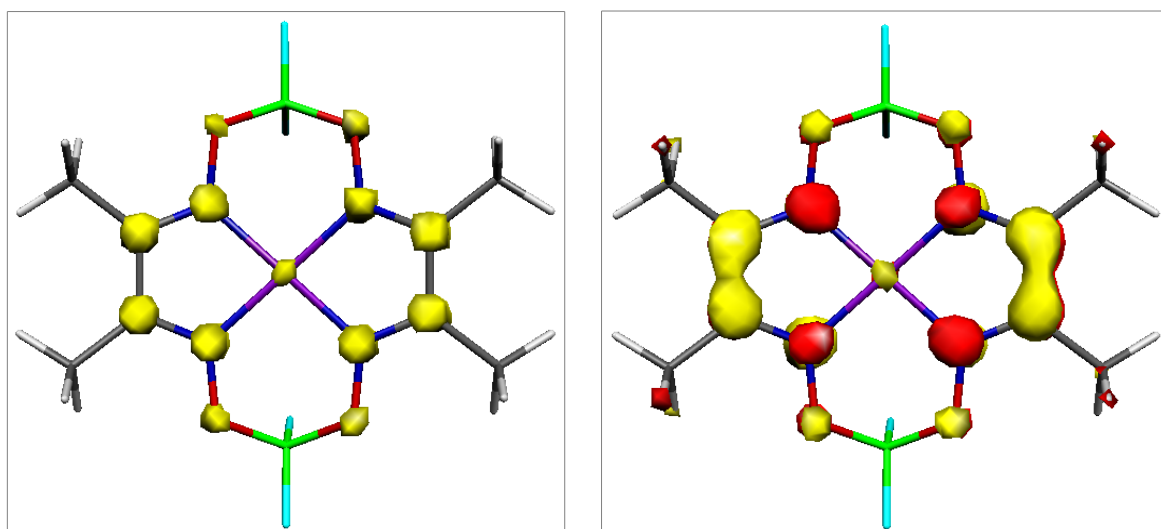


Fig. S11 Spin density plot (left) and localized SOMO (right) for the monoreduced species $[\text{Ni}(\text{DMGBF}_2)_2]^-$.

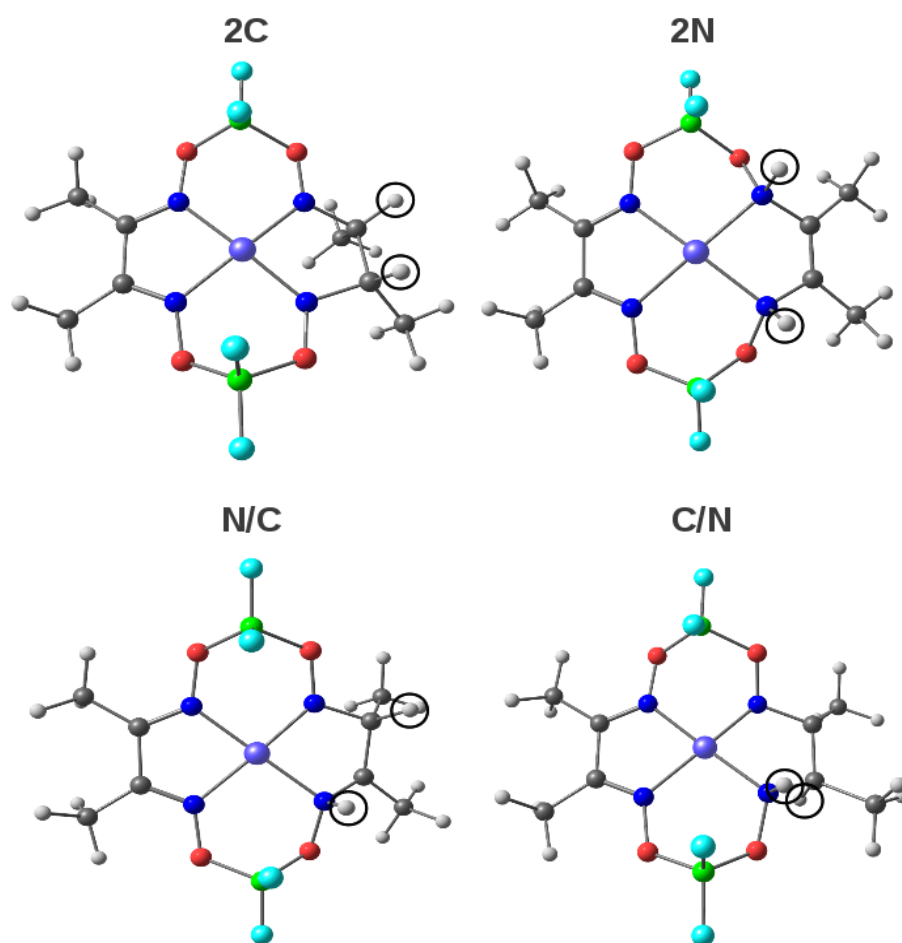


Fig. S12 DFT optimized structures of the doubly protonated species of $[\text{Ni}(\text{DMGBF}_2)_2]^-$.

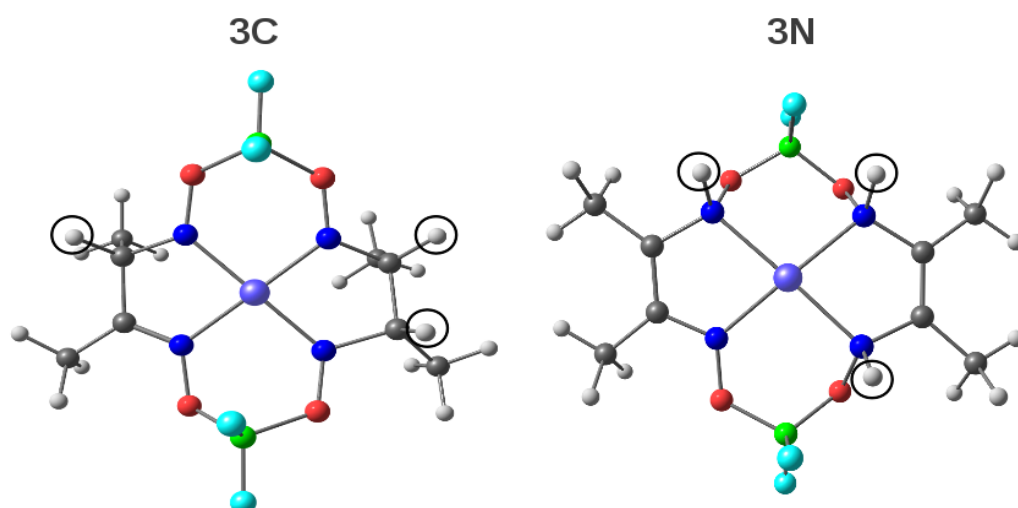


Fig. S13 DFT optimized structures of the triply protonated species of $[\text{Ni}(\text{DMGBF}_2)_2]^-$.

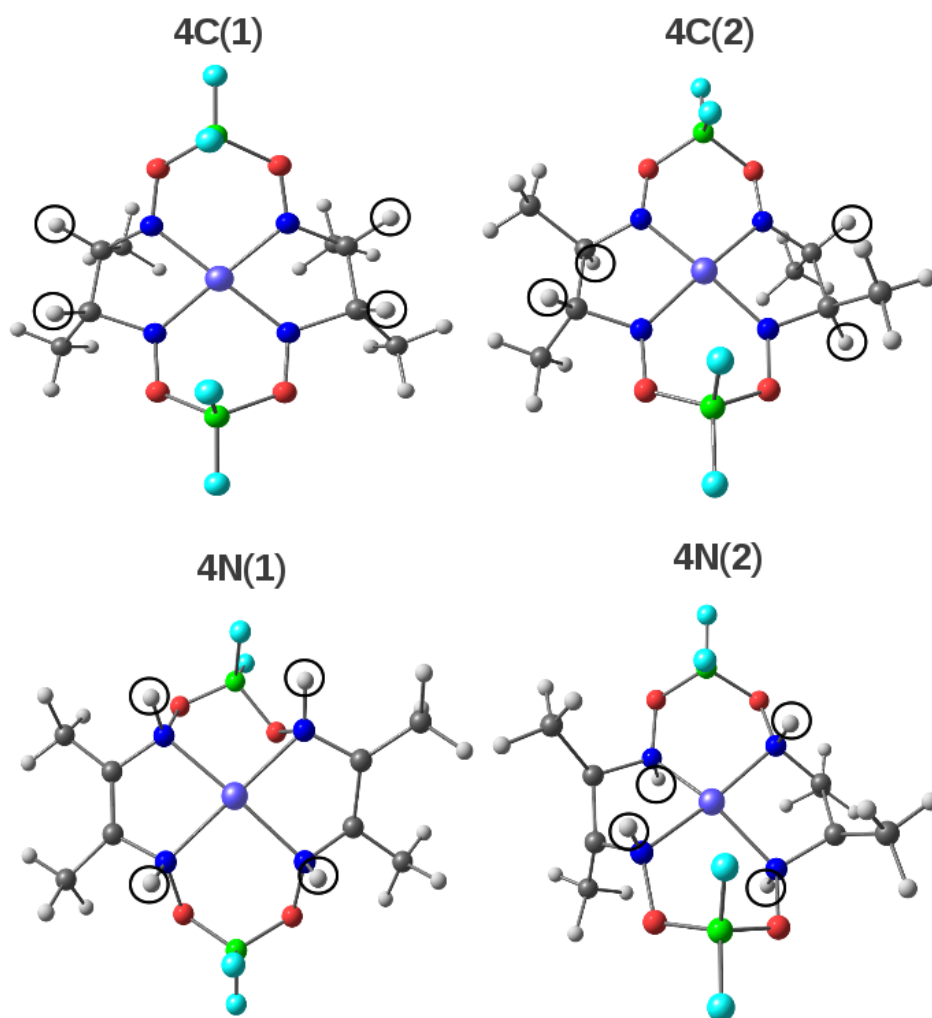


Fig. S14 DFT optimized structures of the quaduply protonated species of $[\text{Ni}(\text{DMGBF}_2)_2]^-$